

Rectangular Photonic Crystal Nanobeam Cavities in Bulk Diamond

Sara Mouradian,^{1,*} Noel H. Wan,^{1,*} Tim Schröder,² and Dirk Englund^{1,†}

¹*Department of Electrical Engineering and Computer Science, Massachusetts Institute of Technology, Cambridge MA 02139*

²*Niels Bohr Institute, University of Copenhagen, 2100 Copenhagen, Denmark*

We demonstrate the fabrication of photonic crystal nanobeam cavities with rectangular cross section into bulk diamond. In simulation, these cavities have an unloaded quality factor (Q) of over 1×10^6 . Measured cavity resonances show fundamental modes with spectrometer-limited quality factors $\geq 14 \times 10^3$ within 1 nm of the NV center's zero phonon line at 637 nm. We find high cavity yield across the full diamond chip with deterministic resonance trends across the fabricated parameter sweeps.

A central aim of quantum information science is the efficient generation of large entangled states of stationary quantum memories with high-fidelity single and two-qubit gates. Among solid-state qubits, a leading system consists of the nitrogen vacancy (NV) center in diamond. Recently, entanglement between distant NV nodes has been demonstrated via single-photon measurements of the zero phonon line (ZPL) emission [1, 2]. Such heralded entanglement can be used to build large cluster states which are a resource for universal quantum computation [3] or quantum repeater networks [4, 5]. However, the coherent ZPL optical transition of the NV accounts for only 3% of the emission due to phonon interactions even at cryogenic temperatures. This severely limits the entanglement rate, even with broadband collection enhancement structures such as a solid immersion lens [2]. To improve the entanglement rate, the collection rate into the desired frequency and spatial mode must be increased. Much recent work has focused on maximizing the coherent ZPL collection efficiency via the Purcell effect in a photonic crystal nanocavity.

One major challenge in coupling the NV to a nanocavity is that high-quality diamond cannot currently be grown in thin (wavelength-scale) waveguiding membranes. Hybrid structures have been used to enhance the ZPL emission [6–8], though the maximum enhancement rate is limited as the NV must be placed out of the cavity's mode maximum. Advances in diamond patterning have enabled the fabrication of photonic crystal cavities in diamond [9] with two main methods: fabrication into thinned diamond membranes [10–17] and angled etching of bulk diamond [18–21]. However, the measured quality (Q) factors have been limited to a few thousand near the NV ZPL. Low cavity yield or inconsistency across the diamond substrate also presents a major scaling challenges, especially for membrane-based approaches.

Recently, Khanaliloo et al. [22, 23] introduced a technique to undercut lithographically defined structures in bulk diamond, allowing for the fabrication of high quality free-standing diamond optomechanical devices. In this Letter, we apply a similar isotropic undercut pro-

cess to the fabrication of photonic crystal nanobeam cavities. Figure 1(a) shows a schematic of the rectangular nanobeam photonic crystal fabricated from bulk diamond. We find that the quasi-isotropic etching procedure is highly repeatable and consistent across the full chip. In addition, the process requires minimal fabrication optimization as electron-beam lithography determines all parameters except for the nanobeam height, which can be precisely tuned during the relatively slow, isotropic etching. This fabrication process enables instrument-limited optical quality (Q) factors exceeding 14,000 within 1 nm of the NV⁻ center ZPL wavelength of 637 nm, as well as uniform nanocavity fabrication across a full chip.

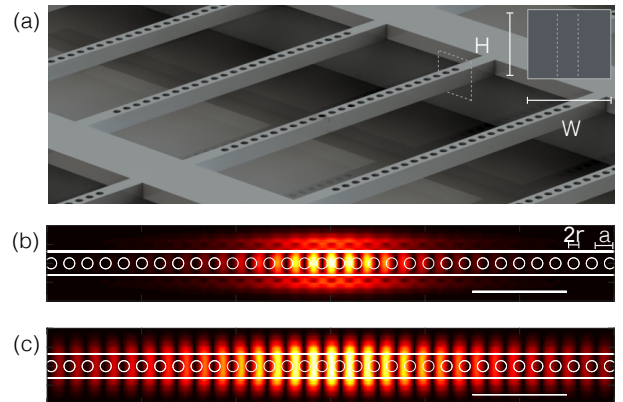


FIG. 1. (a) Schematic of an array of rectangular nanobeam cavities fabricated from bulk diamond. (b) $\text{Re}(E)$ for the first order TE mode. (c) $\text{Re}(E)$ for the first order TM mode. Scale bar for (b) and (c): 1 μm

We design photonic crystal nanobeam cavities to support a low-mode-volume (V) mode with high quality factor Q at the NV ZPL (637 nm), and with the electric-field maximum concentrated in the diamond. The design process begins with approximate cavity parameters derived from band structure simulations and optimizes the cavity Q of the lowest order TE mode (intensity profile shown in Figure 1(b)) at $\lambda_{\text{NV}} = 637 \text{ nm}$ by Finite Difference Time Domain (FDTD) simulations. The final design consists of a diamond waveguide ($W = 250 \text{ nm}$

* S.M. and N.H.W. contributed equally to this work

† englund@mit.edu

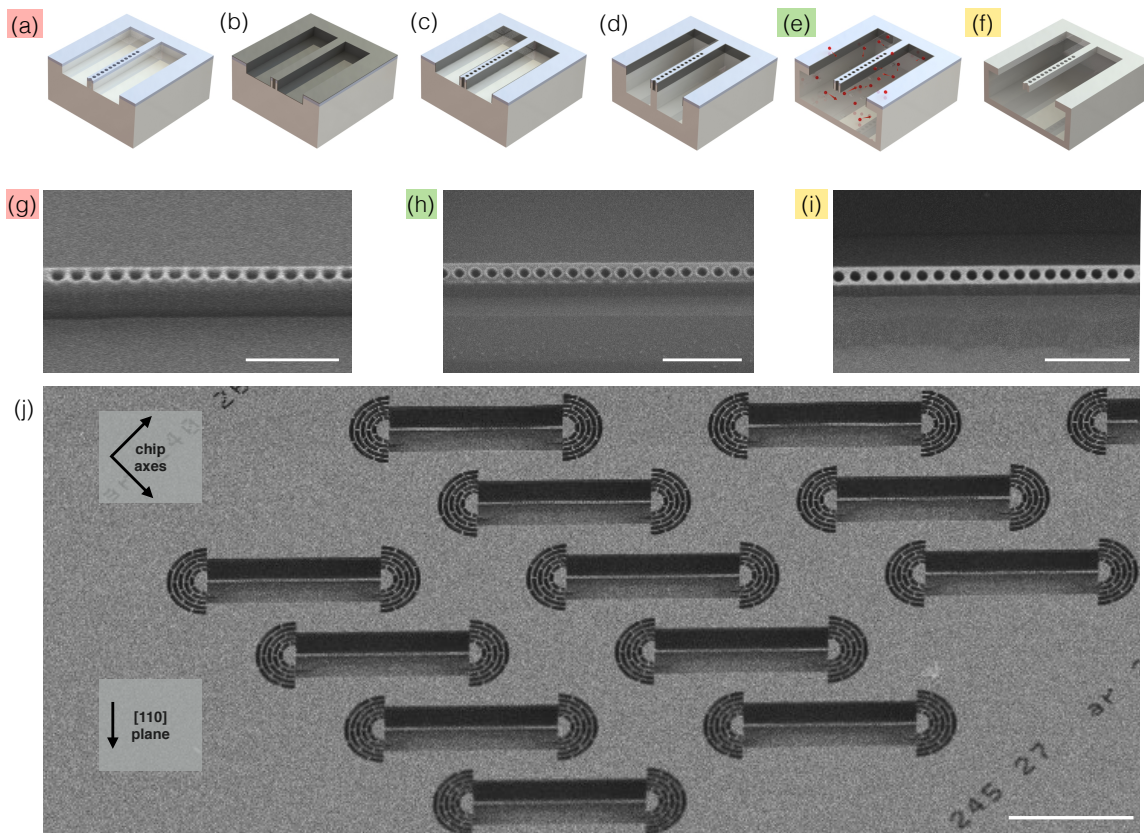


FIG. 2. (a-f) Fabrication steps for rectangular nanobeam photonic crystal cavities, where white, blue, and gray indicate bulk diamond, SiN, and Al_2O_3 , respectively. (a) Anisotropic etch into diamond with SiN hard mask following electron-beam lithography. (b) Atomic layer deposition of Al_2O_3 . (c) Selective removal of the top layer of Al_2O_3 . (d) Anisotropic etch into diamond (e) Quasi-isotropic etch of diamond nanobeam cavity (f) Suspended nanobeam cavity following mask removal. Scanning electron micrographs (g),(h),(i) correspond to processes (a),(e) and (f), respectively. Scale bar: $1\ \mu\text{m}$ (j) Overview of an array of photonic crystal nanobeam cavities. Scale bar: $10\ \mu\text{m}$

and $H = 230\ \text{nm}$) periodically patterned with holes with radius $r = 58\ \text{nm}$ and spacing $a = 192\ \text{nm}$. The defect supporting the cavity mode is introduced by linearly decreasing the hole spacing to $a = 171\ \text{nm}$ over 5 periods. With 25 holes on either side of the cavity region, this cavity has a radiation-limited Q factor of > 1 million. The cavity also supports a TM mode (Figure 1(c) shows the intensity profile) at $615\ \text{nm}$ with a Q of 13,000 in simulation, as well as other TE modes with mode maxima in the outer hole regions with lower Q values – 5,500 and 2,500 in simulation at $649\ \text{nm}$ and $653\ \text{nm}$ respectively. These higher order modes are denoted as M3 and M4 in the measured spectra in Figures 3 and 4.

We fabricated these nanobeam cavity designs in a $3\ \text{mm} \times 3\ \text{mm} \times 0.3\ \text{mm}$ single-crystal diamond with a $\{100\}$ top face grown by chemical vapor deposition (CVD, Element6) with a nitrogen defect density of less than 1 ppm, and thus a native NV density of approximately 1 ppb. High-resolution X-ray diffraction confirmed the crystal orientation to align the nanobeams along the facet with the fastest etch rate ($\{110\}$), which

is 45° from the diamond chip facets on all measured diamond, as illustrated in Fig 2(j). The quasi-isotropic etch rate is facet-dependent [23], and ensures that the beam has a rectangular cross-section. Unlike nanobeam cavities with triangular cross sections which mix the TE and TM modes, these cavities have low out-of-plane scattering loss [18, 20].

Fig. 2(a-f) outlines the essential steps of the fabrication process. A $180\ \text{nm}$ -thick low-stress SiN layer, deposited with plasma-enhanced chemical vapor deposition, functions as a hard mask to pattern the diamond. We observed a selectivity of approximately 30:1 for the oxygen anisotropic etch parameters described below. Electron-beam lithography defines the nanobeam cavities (ZEP 520A exposed at $500\ \mu\text{C}/\text{cm}^2$ and developed at 0°C in ortho-xylene for 90 s). Following resist development, a tetrafluoromethane (CF_4) plasma reactive-ion etch step transfers the pattern into the the SiN hard mask. This pattern is transferred into the diamond (Figure 2(a) using an inductively coupled oxygen plasma (ICP) with a working pressure of $0.15\ \text{Pa}$ with ICP and RF powers of

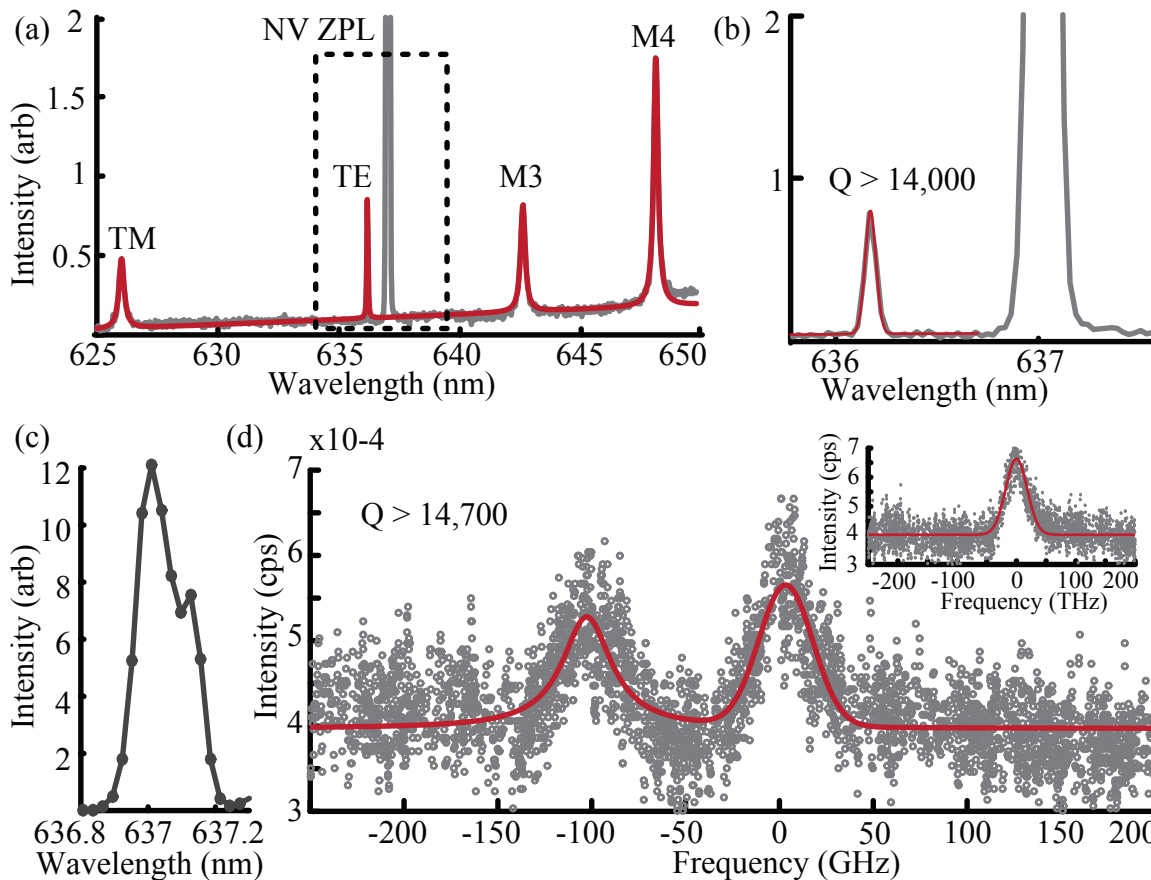


FIG. 3. (a) PL spectrum of Cavity A with lowest order TE and TM cavity peaks fit with Lorentzian functions. (b) Zoom in of the fundamental TE mode of Cavity A. The red line shows a fit to the spectrometer-limited cavity peak, fit with a pseudo-Voigt function. (c) PL spectrum of Cavity B showing the inhomogeneously broadened ZPL emission from the ensemble of excited NVs at 637 nm and a cavity peak at 637.1 nm. (d) Photoluminescence excitation (PLE) spectrum of Cavity B showing a PLE peak at NV ZPL position and a cavity-enhanced PLE peak 100 GHz detuned center from the inhomogeneous ZPL distribution. The inset shows a PLE measurement of the same nanobeam 7 μm from the cavity center showing only the inhomogeneous distribution of NV centers in the sample.

500 W and 240 W, respectively. This anisotropic etch step is 2.5 times as deep as the final desired cavity height for precise tuning of the nanobeam height in the subsequent isotropic undercut etch step. This step produces smooth and straight sidewalls as seen in the scanning electron micrograph (SEM) in Fig. 2(g).

A conformal layer of 20 nm of aluminum oxide (Al_2O_3) produced by atomic layer deposition (ALD), see Fig. 2(b), protects all sides of the nanobeam cavity for the subsequent etch steps. A CF_4 reactive ion etch removes the top Al_2O_3 layer, leaving only the sides covered, as shown in Fig. 2(c). A second anisotropic oxygen etch, using the same parameters as above, removes an additional 1 μm of diamond, as shown in Fig. 2(d). A quasi-isotropic etch then undercuts the nanobeam structure at 200°C and 3 Pa with 900 W ICP and no forward bias (Fig. 2(e)). The elevated temperature and pressure increase the chemical interaction rate with the diamond to increase the etch rate. As seen in the SEM in Fig. 2(h),

the Al_2O_3 is thin enough to allow periodic SEM measurements of the nanobeam height. Once the desired nanobeam height of 230 nm (~ 85 minutes with an initial beam height of 575 nm) and undercut are achieved, the residual SiN and Al_2O_3 are removed using 49% hydrofluoric acid (Fig. 2(f)). An SEM of the final structure after mask removal is shown in Fig. 2(i). The measured chip contains 125 cavities, with 5 copies at each of 25 parameters. The parameter sweep modified the beam widths and hole radii by $\pm 4\%$ and $\pm 16\%$ respectively, to cover a large wavelength range.

We measured the fabricated cavities at 4 K by photoluminescence (PL) and photoluminescence excitation (PLE) spectroscopy. The native population of NV centers, excited using a 532 nm laser, provides an internal light source for the cavity. The cavity PL is collected with a 0.9 NA objective and resolved on a spectrometer with a resolution of 0.06 nm ($Q \sim 14,000$). Fig. 3 shows two cavity spectra: Cavity A ($W = 260$ nm, $r = 55$ nm)

and Cavity B ($W = 245$ nm, $r = 58$ nm). Fig. 3(a) shows the cavity-modified PL spectrum of the NV ensemble at Cavity A under 532 nm excitation. Four modes appear in the spectrum, corresponding to the first-order TE and TM modes (profiles shown in Figure 1(b,c)), as well as the higher-order modes, M3 and M4. Fig. 3(b) shows the high- Q first-order TE mode at 636.1 nm, as well as the inhomogeneously-broadened ZPL of the excited ensemble of NV centers at 637 nm. The linewidth of the cavity mode is limited by the spectrometer’s resolution, as confirmed by comparing to the spectrum of a sub-0.5 MHz laser at the same wavelength. Fitting the spectrum with a pseudo-Voigt function [24] takes into account the effect of the Gaussian spectrometer result on the Lorentzian cavity spectrum. This fit indicates a lower bound of $Q \geq 16700$, above the resolution of the spectrometer ($Q \geq 14,000$).

The spectrum of Cavity B (Fig. 3(c)) reveals the first-order TE mode overlapping with the inhomogeneous distribution of ZPLs in the NV ensemble. We performed PLE spectroscopy to better measure the Q of this cavity and study the cavity-enhanced excitation of the NV ensemble. The PLE consisted of NV phonon side band (PSB) detection (filtered > 650 nm) while scanning a < 0.5 MHz-linewidth laser over the NV ZPL and cavity frequencies. The inset of Fig. 3(c) shows the PLE spectrum of the unpatterned nanobeam $7 \mu\text{m}$ from the cavity center. This reveals an inhomogeneously broadened absorption spectrum of the excited population of NV centers centered at 470.48 THz (637.2 nm) with a full width half maximum of 42.7 GHz. A PLE scan at the center of the cavity shows a second peak that is absent on the rest of the sample; we attribute this to the cavity-enhanced absorption of NV centers coupled to the cavity mode. A Lorentzian fit of the peak reveals a measured cavity Q of 14,700. This provides a lower bound on the Q of the bare cavity mode, as the PLE spectrum may be broadened by the interaction with the inhomogeneous distribution of emitters coupled to this mode of the cavity [25].

A survey of all of the fabricated devices demonstrates the consistency and high yield of our fabrication technique. Fig. 4(a) shows the measured cavity resonances of mode M4 across the full range of parameters. The error bars show the standard deviation of the wavelength position for the 5 cavities fabricated with each parameter set. We used here mode M4 as it has the highest vertical loss of the four modes considered here, and thus the highest SNR in spectrometer measurements. This survey reveals the expected trends: the resonance wavelengths increase with larger beam widths and decrease with larger holes radii. The standard deviation within each parameter is low with an average of ± 2.2 nm deviation from the mean in each parameter set, showing the consistency of the fabrication process. The spectra of M3 and M4 of the 5 cavities with $W = 260$ nm and

$r = 58$ nm (circled in Fig. 4(a)) are shown in Fig. 4(b).

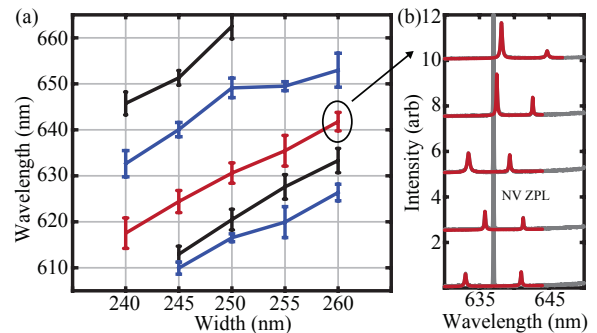


FIG. 4. (a) Frequency distribution of resonant frequencies of Mode 4 for all 25 sets of parameters. The error bars show the standard deviation $\pm\sigma$ of the resonant frequencies for the 5 cavities fabricated for each set of parameters. (b) The spectra of the 5 cavities fabricated with $W = 260$ nm and $r = 58$ nm (circled in (a)) showing the distribution of M3 and M4.

In summary, we have demonstrated a method to fabricate high- Q photonic crystal nanobeam cavities from bulk diamond at the NV ZPL wavelength. We measured cavity resonances within 1 nm of the NV ZPL wavelength, with instrument-limited Q factors larger than 14,000. The process showed consistent cavity properties across all fabricated devices. Future work will apply this fabrication process to high-purity diamond with a nitrogen concentration below 100 ppb, which should enable the coupling of individual NV ZPLs with high Purcell enhancement. The rectangular cross section of these cavities should enable efficient mode conversion between diamond waveguides and on-chip ridge or channel waveguides [26]. This fabrication technique applies to other diamond color centers, such as the germanium vacancy and silicon vacancy centers. These emitters have naturally narrow emission linewidth [27] so that the nanocavity parameters achieved here should allow for the strong coupling regime of cavity quantum electrodynamics.

ACKNOWLEDGMENTS

This research was supported in part by the Army Research Laboratory Center for Distributed Quantum Information (CDQI). S.M. was supported in part by the NSF IQuISE program and the NSF program ACQUIRE: “Scalable Quantum Communications with Error-Corrected Semiconductor Qubits.” N.W. was supported by CDQI.

-
- [1] Emre Togan, Yiwen Chu, AS Trifonov, Liang Jiang, Jeronimo Maze, Lilian Childress, MV Gurudev Dutt, Anders Søndberg Sørensen, PR Hemmer, AS Zibrov, *et al.*, “Quantum entanglement between an optical photon and a solid-state spin qubit,” *Nature* **466**, 730–734 (2010).
- [2] H Bernien, B Hensen, W Pfaff, G Koolstra, M S Blok, L Robledo, T H Taminiau, M Markham, D J Twitchen, L Childress, and R Hanson, “Heralded entanglement between solid-state qubits separated by three metres,” *Nature* **497**, 86–90 (2013).
- [3] Sean D Barrett and Pieter Kok, “Efficient high-fidelity quantum computation using matter qubits and linear optics,” *Physical Review A* **71**, 060310 (2005).
- [4] L Childress, JM Taylor, Anders Søndberg Sørensen, and Mikhail D Lukin, “Fault-tolerant quantum repeaters with minimal physical resources and implementations based on single-photon emitters,” *Physical Review A* **72**, 052330 (2005).
- [5] Scott E Vinay and Pieter Kok, “Practical repeaters for ultra-long distance quantum communication,” arXiv preprint arXiv:1607.08140 (2016).
- [6] Michael Gould, Emma R Schmidgall, Shabnam Dadgostar, Fariba Hatami, and Kai-Mei C Fu, “Efficient extraction of zero-phonon-line photons from single nitrogen-vacancy centers in an integrated gap-on-diamond platform,” *Physical Review Applied* **6**, 011001 (2016).
- [7] Dirk Englund, Brendan Shields, Kelley Rivoire, Fariba Hatami, Jelena Vuckovic, Hongkun Park, and Mikhail D Lukin, “Deterministic coupling of a single nitrogen vacancy center to a photonic crystal cavity,” *Nano letters* **10**, 3922–3926 (2010).
- [8] Janik Wolters, Andreas W Schell, Günter Kewes, Nils Nüsse, Max Schoengen, Henning Döscher, Thomas Hannappel, Bernd Löchel, Michael Barth, and Oliver Benson, “Enhancement of the zero phonon line emission from a single nitrogen vacancy center in a nanodiamond via coupling to a photonic crystal cavity,” *Applied Physics Letters* **97**, 141108 (2010).
- [9] Tim Schröder, Sara L Mouradian, Jiabao Zheng, Matthew E Trusheim, Michael Walsh, Edward H Chen, Luozhou Li, Igal Bayn, and Dirk Englund, “Quantum nanophotonics in diamond [invited],” *JOSA B* **33**, B65–B83 (2016).
- [10] Andrei Faraon, Paul E Barclay, Charles Santori, Kai-Mei C Fu, and Raymond G Beausoleil, “Resonant enhancement of the zero-phonon emission from a colour centre in a diamond cavity,” *Nature Photonics* **5**, 301–305 (2011).
- [11] Andrei Faraon, Charles Santori, Zhihong Huang, Victor M Acosta, and Raymond G Beausoleil, “Coupling of nitrogen-vacancy centers to photonic crystal cavities in monocrystalline diamond,” *Physical review letters* **109**, 033604 (2012).
- [12] BJM Hausmann, BJ Shields, Q Quan, Y Chu, NP De Leon, R Evans, MJ Burek, AS Zibrov, M Markham, DJ Twitchen, *et al.*, “Coupling of nv centers to photonic crystal nanobeams in diamond,” *Nano letters* **13**, 5791–5796 (2013).
- [13] Jonathan C Lee, David O Bracher, Shanying Cui, Kenichi Ohno, Claire A McLellan, Xingyu Zhang, Paolo Andrich, Benjamin Alemán, Kasey J Russell, Andrew P Magyar, *et al.*, “Deterministic coupling of delta-doped nitrogen vacancy centers to a nanobeam photonic crystal cavity,” *Applied Physics Letters* **105**, 261101 (2014).
- [14] Luozhou Li, Tim Schröder, Edward H Chen, Michael Walsh, Igal Bayn, Jordan Goldstein, Ophir Gaathon, Matthew E Trusheim, Ming Lu, Jacob Mower, *et al.*, “Coherent spin control of a nanocavity-enhanced qubit in diamond,” *Nature communications* **6** (2015).
- [15] Janine Riedrich-Möller, Carsten Arend, Christoph Pauly, Frank Mücklich, Martin Fischer, Stefan Gsell, Matthias Schreck, and Christoph Becher, “Deterministic coupling of a single silicon-vacancy color center to a photonic crystal cavity in diamond,” *Nano letters* **14**, 5281–5287 (2014).
- [16] Janine Riedrich-Möller, Laura Kipfstuhl, Christian Hepp, Elke Neu, Christoph Pauly, Frank Mücklich, Armin Baur, Michael Wandt, Sandra Wolff, Martin Fischer, Stefan Gsell, Matthias Schreck, and Christoph Becher, “One- and two-dimensional photonic crystal microcavities in single crystal diamond,” *Nature Nanotechnology* **7**, 69–74 (2012).
- [17] Luozhou Li, Igal Bayn, Ming Lu, Chang-Yong Nam, Tim Schröder, Aaron Stein, Nicholas C Harris, and Dirk Englund, “Nanofabrication on unconventional substrates using transferred hard masks,” *Scientific reports* **5** (2015).
- [18] Igal Bayn, Boris Meyler, Joseph Salzman, and Rafi Kalish, “Triangular nanobeam photonic cavities in single-crystal diamond,” *New Journal of Physics* **13**, 025018 (2011).
- [19] Igal Bayn, Sara Mouradian, Luozhou Li, Jordan A. Goldstein, Tim Schröder, Jiabao Zheng, Ed H. Chen, Ophir Gaathon, Ming Lu, Aaron Stein, Carl A. Ruggiero, J Salzman, R Kalish, and Dirk Englund, “Fabrication of triangular nanobeam waveguide networks in bulk diamond using single-crystal silicon hard masks,” *Applied Physics Letters* **105**, 211101 (2014).
- [20] Michael J Burek, Yiwen Chu, Madelaine SZ Liddy, Parth Patel, Jake Rochman, Srujan Meesala, Wooyoung Hong, Qimin Quan, Mikhail D Lukin, and Marko Lončar, “High quality-factor optical nanocavities in bulk single-crystal diamond,” *Nature communications* **5** (2014).
- [21] M Schukraft, J Zheng, T Schröder, SL Mouradian, M Walsh, ME Trusheim, H Bakhru, and DR Englund, “Invited article: Precision nanoimplantation of nitrogen vacancy centers into diamond photonic crystal cavities and waveguides,” *APL Photonics* **1**, 020801 (2016).
- [22] Behzad Khanaliloo *et al.*, “High-q/v monolithic diamond microdisks fabricated with quasi-isotropic etching,” *Nano letters* **15**, 5131–5136 (2015).
- [23] Behzad Khanaliloo *et al.*, “Single-crystal diamond nanobeam waveguide optomechanics,” *Physical Review X* **5**, 041051 (2015).
- [24] Roland Albrecht, Alexander Bommer, Christian Deutsch, Jakob Reichel, and Christoph Becher, “Coupling of a single nitrogen-vacancy center in diamond to a fiber-based microcavity,” *Physical review letters* **110**, 243602 (2013).
- [25] Daniel Valente, Jan Suffczyński, Tomasz Jakubczyk, Adrien Dousse, Aristide Lemaître, Isabelle Sagnes, Loïc

- Lanco, Paul Voisin, Alexia Auffèves, and Pascale Senellart, “Frequency cavity pulling induced by a single semiconductor quantum dot,” *Physical Review B* **89**, 041302 (2014).
- [26] Sara L Mouradian, Tim Schröder, Carl B Poitras, Luozhou Li, Jordan Goldstein, Edward H Chen, Michael Walsh, Jaime Cardenas, Matthew L Markham, Daniel J Twitchen, *et al.*, “Scalable integration of long-lived quantum memories into a photonic circuit,” *Physical Review X* **5**, 031009 (2015).
- [27] Tim Schröder, Matthew E Trusheim, Michael Walsh, Luozhou Li, Jiabao Zheng, Marco Schukraft, Jose L Pacheco, Ryan M Camacho, Edward S Bielejec, Alp Sipahigil, *et al.*, “Scalable focused ion beam creation of nearly lifetime-limited single quantum emitters in diamond nanostructures,” arXiv preprint arXiv:1610.09492 (2016).